# We are IntechOpen, the world's leading publisher of Open Access books Built by scientists, for scientists

**4,800**
Open access books available

**122,000**
International authors and editors

**135M**
Downloads

Our authors are among the

**154**
Countries delivered to

**TOP 1%**
most cited scientists

**12.2%**
Contributors from top 500 universities


WEB OF SCIENCE™

Selection of our books indexed in the Book Citation Index in Web of Science™ Core Collection (BKCI)

## Interested in publishing with us?
## Contact book.department@intechopen.com

Numbers displayed above are based on latest data collected.
For more information visit www.intechopen.com

Chapter 1

# Generation of High-Intensity Laser Pulses and their Applications

Tae Moon Jeong and Jongmin Lee

Additional information is available at the end of the chapter

http://dx.doi.org/10.5772/64526

**Abstract**

The progress in the laser technology makes it possible to produce a laser pulse having a peak power of over PW. Focusing such high-power laser pulses enables ones to have unprecedentedly strong laser intensity. The laser intensity over $10^{19}$ W/cm$^2$, which is called the relativistic laser intensity, can accelerate electrons almost to the speed of light. The acceleration of charged particles using such a high-power laser pulse has been successfully demonstrated in many experiments. According to the recent calculation using the vector diffraction theory, it is possible, by employing a tight focusing geometry, to produce a femtosecond (fs) laser focal spot to have an intensity of over $10^{24}$ W/cm$^2$ in the focal plane. Over this laser intensity, protons can be directly accelerated almost to the speed of light. Such ultrashort and ultrastrong laser intensities will bring ones many opportunities to experimentally study ultrafast physical phenomena we have never met before. This chapter describes how to generate a high-power laser pulse. And, then the focusing characteristics of a femtosecond high-power laser pulse are discussed in the scalar and the vector diffraction limits. Finally, the applications of ultrashort high-power laser are briefly introduced.

**Keywords:** ultrashort laser pulse, high-intensity laser pulse, chirped pulse amplification, charged particle acceleration, tight focusing

## 1. Generation of ultrashort laser pulses

Femtosecond (fs) high-power laser pulses having a peak power of PW or higher are being produced for the study of laser-matter interactions in the relativistic intensity regime. An ultrashort laser pulse is generated in a mode-locked laser oscillator in the front and its energy is amplified in the following amplifiers. The mode locking is a technique to produce laser

pulses having a pulse duration in the ultrashort time scale such as picosecond (ps) or fs [1, 2]. In the technique, a gain or a loss of an oscillator is modulated in an active or a passive manner. Saturable absorber is a typical optical element modulating a loss in an oscillator. Nonlinear effect dependent on the laser intensity is used to realize a saturable absorption instantaneously responding to the intensity. Under the saturable absorption, a laser pulse experiences a lower loss at a higher intensity. As a result, a higher intensity part of a laser pulse grows much stronger and the temporal duration becomes shorter during the saturable absorption process.

As the pulse duration of a laser pulse decreases, the spectrum of the pulse becomes broader and the pulse encounters the dispersion effect in the medium. The dispersion effect frequently tends to broaden the pulse duration. Without any dispersion control device, the resultant pulse duration is determined by the balance between the pulse shortening due to the saturation absorption and the pulse broadening due to the dispersion. With a proper dispersion control device, the dispersion in a laser pulse is compensated and the pulse duration is mostly determined by the spectral bandwidth of the laser pulse. The minimum pulse duration obtainable with a spectral bandwidth is known as the transform-limited pulse duration. Up to date, sub-10 fs laser pulses from an oscillator are generated by compensating for the dispersion effect with prism pairs [3]. In this section, the basic principle of the mode-locking technique is explained for generating an ultrashort laser pulse and the formation of an ultrashort laser pulse is described.

### 1.1. Short pulse generation by locking phase of longitudinal mode

When a laser oscillator is formed with an optical length of $L$, the wavelength of standing waves inside the oscillator is determined by $2L/m$ ($m$ is a positive integer), and alternatively, the frequency by $\nu_m = m \times c/2L$ (or $\omega_m = m \times \pi c/L$). The oscillating frequency in the oscillator is limited by a gain spectrum and it is called the longitudinal mode of the oscillator. A laser pulse can be decomposed into the summation of each electric field having different modes, and the resultant electric field of the pulse can be written as a superposition of oscillating modes:

$$E(z,t) = \sum_m E_m \exp\left\{ i\omega_m \left( t - \frac{z}{c} \right) \right\}. \tag{1}$$

In a free running laser, the phase relation among oscillating modes is random and this is the origin of a short-timescale random intensity fluctuation. The phase relation between modes can be constant (i.e., $\nu_m - \nu_{m-1}$ = constant) under a specific condition. The situation of having the constant phase relation between modes is mentioned as "mode-locked." In this case, the intensity of the resultant electric field is given by

$$I(z,t) = \left|E(z,t)\right|^2 = \left|E_0(z,t)\right|^2 \frac{\sin^2\left\{ m\omega_m \left( t - z/c \right)/2 \right\}}{\sin^2\left\{ \omega_m \left( t - z/c \right)/2 \right\}}. \tag{2}$$

As can be seen in Eq. (2), a strong intensity peak can grow in the resonator when oscillating electric fields are added under the mode-locking condition. This is the basic principle for generating a mode-locked laser pulse (see **Figure 1**). As expected in Eq. (2), the pulse duration of a mode-locked laser pulse is determined by the number of oscillating modes. For example, a Ti:sapphire laser that typically produces 10-fs laser pulses contains several hundred-thousand modes in the spectral bandwidth. Up to date, a number of mode-locking techniques have been introduced to generate ps and fs laser pulses, but the underlying physics is basically the same and the question is how to realize locking longitudinal modes.

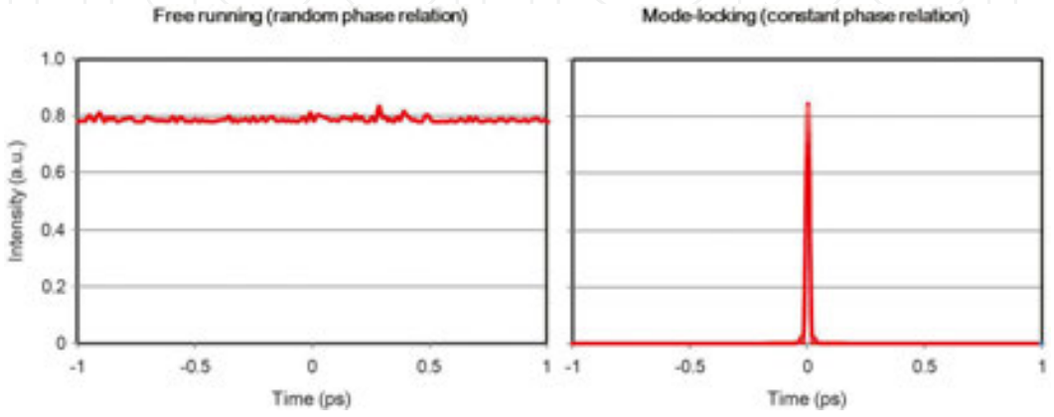


**Figure 1.** Power at free running and mode-locked operations. When the phase relation is random among longitudinal modes, the intensity has fluctuation because of the beating among modes (left). On the other hand, a single high peak laser pulse is formed under the constant phase relation between modes (right).

### 1.2. How to lock phases of longitudinal modes

In the early history of mode-locking technique, an active loss element operating at an rf-frequency was installed in an oscillator. The element periodically inducing intensity loss initiates an intensity modulation at a repetition rate corresponding to the round-trip time. A periodic loss at a round-trip time forces to form a laser pulse inside the oscillator. This is known as the active mode-locking technique. Another technique is to introduce a passive-type intensity modulation to the oscillator. Thus, in the passive mode-locking technique, an optical element that has an intensity-dependent loss is installed in the oscillator. The intensity peak in the temporal domain has higher transmittance and energy gain, but a lower intensity part has lower transmittance and energy gain. The lower intensity part is relatively suppressed by the intensity-dependent loss when an intensity fluctuation circulates in the oscillator. As the intensity peak grows, the number of oscillating modes becomes larger and larger in the spectral domain, and the phase relation between modes is automatically locked to form a laser pulse.

#### *1.2.1. Saturable absorption*

Some materials have a property that the absorption of light decreases as increasing the light intensity. This kind of material is known as the saturable absorber. In the saturable absorber, the light propagating in the medium transfers its energy to electrons in the ground level and

excites them to higher energy levels. The light intensity decreases as the light propagates in the medium. The light absorption becomes very weak when the number of electrons in the ground level becomes sufficiently low, and the rest of light energy almost transmits the medium. At a time later, the excited electrons spontaneously decay into the ground level and the number of ground electrons is recovered to be ready to absorb energy from light. This phenomenon is known as the saturable absorption. The saturable absorber can be divided into slow and fast saturable absorbers, depending on the recovery time $\tau_r$. In the slow saturable absorber, the recovery time is slower than the pulse duration $\tau_p$ and it is assumed to be shorter than the round-trip time under the mode-locking condition. Most saturable absorbers used as the form of solid state and semiconductor have the slow recovery property. In a slow saturable absorber, the intensity-dependent loss is described as follows:

$$\frac{dL}{dt} = -\frac{L - L_0}{\tau_r} - \frac{I}{F_{sat}} L \,. \tag{3}$$

Here, $L_0$ is the unsaturated loss and $F_{\text{sat}}$ is the saturation fluence. Since $\tau_r \gg \tau_p$, the second term on the right-hand side of Eq. (3), is dominant and the loss exponentially decreases with respect to the pulse fluence $\int_{-\infty}^{t} I(t)dt$. For the slow absorber, two mode-locking regimes are possible depending on the soliton effect. Without the soliton effect, a slow saturable absorber absorbs the leading part of a pulse while the trailing part is less absorbed. The pulse formation is mostly determined by balancing between the net gain and losses. As a result, a pulse profile becomes shortened, and the pulse duration obtainable in this case is estimated by [4]

$$\tau_p = \frac{1.07}{\Delta \nu_g} \sqrt{\frac{g}{\Delta R}} \,. \tag{4}$$

Here, $\Delta\nu_g$ is the FWHM gain bandwidth, assuming a Gaussian-shaped gain spectrum, and $\Delta R$ is the modulation depth. As will be discussed later, the laser pulse can be broadened by the dispersion. Under a proper condition, the shortening and broadening processes can be balanced. Thus, for a slow saturable absorber with the soliton effect, a short laser pulse is generated by the self-phase modulation (SPM) in combination with an appropriate amount of negative dispersion. In this case, the pulse duration can be estimated by [4]

$$\tau_p \approx 1.76 \times \frac{2|D|}{\gamma_{SPM} E_p} \,. \tag{5}$$

Here, $D$ is the group delay dispersion (GDD) per cavity round trip, $\gamma_{\text{SPM}}$ is the SPM coefficient (in rad/W) per round trip, and $E_p$ is the pulse energy. **Figure 2(a)** and **(b)** shows the pulse formation with the slow saturable absorber. The laser pulse is formed when the loss decreases below the gain. The gain can be either unsaturated or saturated during the saturation absorption process. Under the unsaturated gain, the laser pulse gains energy quickly in the beginning

of the saturation absorption process. When the gain is saturated during the saturable absorption, the decrease in the gain is slightly delayed and thus the net gain exists for the pulse formation.

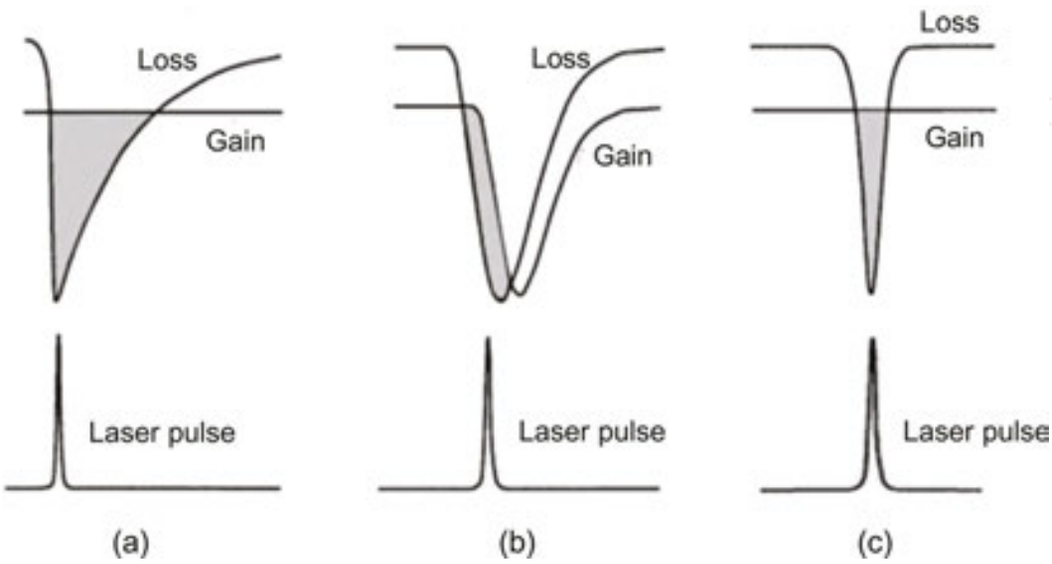


**Figure 2.** Laser pulse formation with saturable absorbers. The gain is not saturated in (a), but the gain is saturated in (b) during the saturation absorption process. (c) The absorption is quickly recovered in the fast saturable absorber. The laser pulse is formed when the loss decreases below the gain.

The absorption by the material is assumed to be instantaneously recovered in the fast saturable absorber (see **Figure 2(c)**). Thus, a higher intensity in the pulse center experiences a higher transmittance and a lower intensity in the side is suppressed by the saturable absorption. When a fast saturable absorber is installed in an oscillator, the intensity of a transmitted laser pulse increases in a gain medium at a growing rate of

$$\frac{dI}{dz} = \frac{g_0 I}{1 + I/I_{sat}}. \tag{6}$$

Here, $I_{sat}$ is the saturation intensity and $g_0$ is the unsaturated small signal gain. Thus, the pulse profile is controlled by the intensity, and a higher gain at a higher intensity leads to the pulse shortening. The pulse duration is given by [5]

$$\tau_p \cong \frac{0.79}{\Delta\nu}\left(\frac{g}{L}\right)^{1/2}\left(\frac{I_{sat}}{I}\right)^{1/2}, \tag{7}$$

with the assumption of a hyperbolic secant pulse profile. Here, $\Delta\nu$ is the gain bandwidth, $g$ is the gain defined by $g_0/(1 + I/I_{sat})$, and $L$ is the saturated loss. In reality, the fast saturable absorbing material operating in the femtosecond regime does not exist. Instead, there are materials having a strong nonlinear effect. These materials can possess the property of ultrafast

loss modulation that is induced by the nonlinear effect. The ultrashort pulse formation by these materials can be considered as the mode locking by the fast saturable absorber. In this section, self-phase modulation as a nonlinear effect which induces ultrafast change in reflection or transmission is discussed.

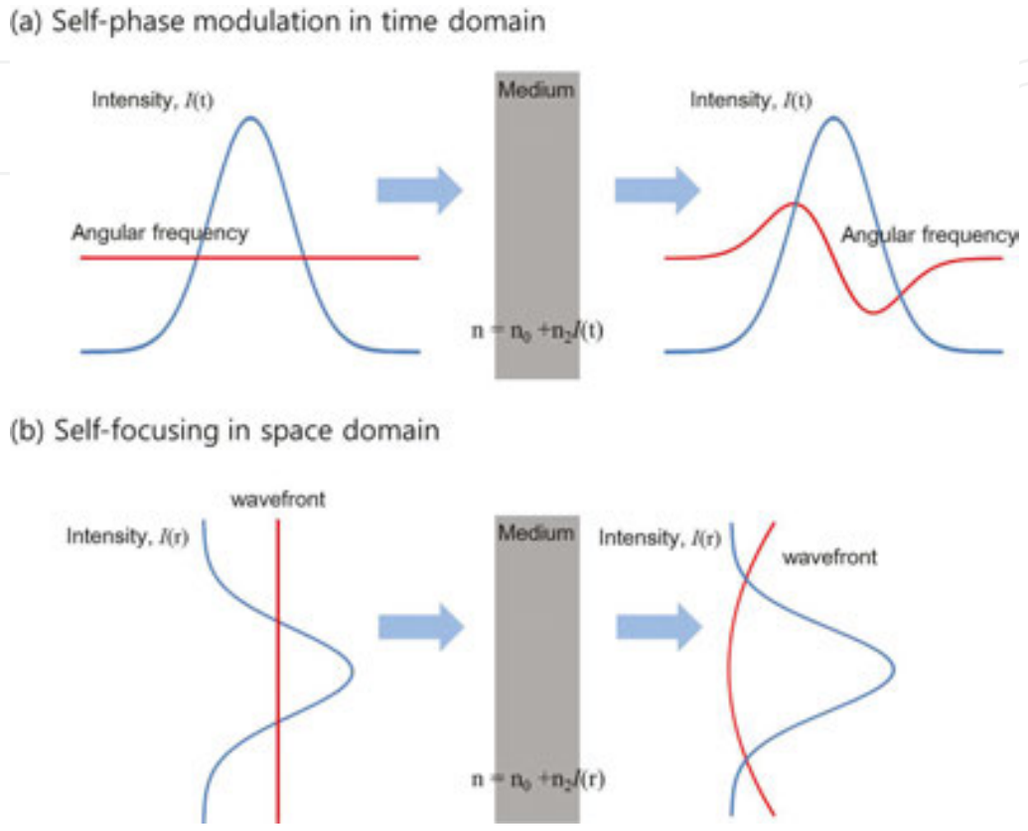


**Figure 3.** (a) Self-phase modulation in time induces the time-dependent phase variation. The lower angular frequency in the rising part and the higher angular frequency in the falling part are induced. (b) Self-phase modulation in space makes the wavefront quadratically curved.

When a light pulse passes through a medium, it experiences an intensity-dependent change in refractive index. This phenomenon is known as the Kerr effect. The Kerr effect can induce an instantaneous loss modulation and make a medium to act as a fast saturable absorber (see **Figure 3**). In order to derive how the Kerr effect is related with the instantaneous loss modulation, let us consider the refractive index depending on the laser intensity which is given by

$$n = n_0 + n_2 I. \tag{8}$$

Here, $n_0$ is the normal refractive index and $n_2$ is the nonlinear refractive index related with the Kerr effect. After a nonlinear medium, the phase of the laser pulse is modified by

$$\phi = nkd = n_0 kd + n_2 Ikd. \tag{9}$$

With a Gaussian pulse profile, $I = I_0 \exp\left(-2t^2/\tau_p^2\right)$, in time, the second term on the right-hand side in Eq. (8) induces time-dependent phase variation, and the angular frequency is calculated as

$$\omega = -\frac{d\phi}{dt} = -\frac{d}{dt}\left(nkd\right) = -n_2 kd\,\frac{dI}{dt} = \frac{4n_2 kdI_0 t}{\tau_p^2}\exp\left(-2t^2/\tau_p^2\right). \tag{10}$$

Thus, after a nonlinear medium, a laser pulse has lower frequency components in the rising edge and higher frequency components in the falling edge. When a Gaussian pulse having these induced frequency components is coherently added to the original one, the constructive interference occurs at the pulse center, but the destructive interference occurs at the edge. The constructive and destructive interferences induce an instantaneous reflectance change in time. This leads to the pulse shortening effect in time. Nonlinear coupled-cavity mode-locking technique introduced as the additive-pulse mode locking (APM) uses the instantaneous reflectance change induced by the self-phase modulation [6].

A similar phenomenon happens in the spatial domain as well. With a Gaussian beam profile, $I = I_0 \exp\left(-2r^2/w_0^2\right)$, in space, the phase at a radial position, $r$, is given by

$$\phi(r) = n_2 kdI(r) = n_2 kdI_0 \exp\left(-2r^2/w_0^2\right) \approx n_2 kdI_0\left(1 - \frac{2r^2}{w_0^2}\right). \tag{11}$$

with an approximation of $\exp\left(-2r^2/w_0^2\right) \approx \left(1 - 2r^2/w_0^2\right)$. The phase variation induced by the nonlinear effect makes the wavefront quadratically curved in the radial direction. This means that, after the nonlinear medium with a positive nonlinear refractive index, the phase at a higher intensity becomes retarded to the phase at a lower intensity. The focal length induced by the quadratic curvature is calculated as

$$f_{nl} = -\frac{dr}{d\phi} = \frac{w_0^2}{4n_2 dI_0}. \tag{12}$$

This phenomenon is known as the self-focusing. Kerr-lens mode-locking (KLM) technique employs the self-focusing to induce an instantaneous intensity-dependent transmittance [7]. In the KLM technique, a higher intensity part can be separated by the self-focusing in combination with an aperture. A higher intensity part in time and space domain has a higher transmittance because of the self-focusing. As a result, a higher intensity grows as a laser pulse circulates in a oscillator. The KLM technique forms an ultrashort pulse using this pulse shortening process. In the technique, a gain medium in the resonator also acts as a nonlinear medium that induces the self-focusing.

### 1.3. Dispersion

When a laser pulse propagates in a material with a length of $d$, the phase is given by the refractive index, $n(\omega)$, of the medium as follows:

$$\phi(\omega) = n(\omega) \cdot k \cdot d = \frac{n(\omega) \cdot \omega \cdot d}{c}. \tag{13}$$

The refractive index of a medium is a function of the angular frequency and can be expressed as the Sellmeier's formula of wavelength as follows:

$$n^2(\lambda) = 1 + \frac{B_1\lambda^2}{\lambda^2 - C_1} + \frac{B_2\lambda^2}{\lambda^2 - C_2} + \frac{B_3\lambda^2}{\lambda^2 - C_3}. \tag{14}$$

with the help of definition, $\lambda = 2\pi c/\omega$. Here, $B_1$, $B_2$, $B_3$, $C_1$, $C_2$, and $C_3$ are known as Sellmeier's coefficients for material. Because of the refractive index of material depending on the wavelength, the phase of an ultrashort laser pulse after material experiences a distortion known as the dispersion. The dispersion is responsible for the broadening of a pulse duration and the distortion of the pulse profile in time. In order to see the effect of dispersion, let us express the spectral phase depending on the angular frequency as the Taylor expansion,

$$\phi(\omega) = \sum_{m=0}^{\infty} (\omega - \omega_0)^m \left.\frac{\partial^m \phi(\omega)}{\partial \omega^m}\right|_{\omega=\omega 0} = \frac{d}{c} \sum_{m=0}^{\infty} (\omega - \omega_0)^m \left.\frac{\partial^m \{\omega \cdot n(\omega)\}}{\partial \omega^m}\right|_{\omega=\omega 0}. \tag{15}$$

Now, we define derivatives as

$$\left.\frac{\partial^n \phi(\omega)}{\partial \omega^n}\right|_{\omega=\omega 0} = \left.\frac{\partial^n \{\omega \cdot n(\omega)\}}{\partial \omega^n}\right|_{\omega=\omega 0} = D_n(\omega = \omega_0). \tag{16}$$

Because the material has a refractive index depending on the frequency, Eqs. (15) and (16) show interesting properties when a laser pulse with a broad spectrum propagates in the material. The first term, $D_0 = d \cdot \omega \cdot n/c$, in the phase relation represents a phase propagation in the material. The second term defined by $D_1(\omega = \omega_0) = \partial\phi(\omega)/\partial\omega|_{\omega=\omega 0}$ is known as the group delay (GD) that can be interpreted as $d/v_g$. Here, $v_g$ is the group velocity and represents the pulse propagation in the material. The third term defined by $D_2(\omega = \omega_0) = \partial^2\phi(\omega)/\partial\omega^2|_{\omega=\omega 0}$ is known as the group delay dispersion (GDD) that is responsible for the temporal broadening of a pulse. The temporal broadening by the group delay dispersion is sometimes known as the chirping which originally means the frequency change in time.

Two kinds of temporal broadenings are possible depending on the sign of $D_2$. When the sign of $D_2$ is positive, a long (red-like) wavelength component travels faster than a blue-like one in the pulse. On the other hand, a short (blue-like) wavelength component travels faster than a red-like one with a negative sign of $D_2$. A pulse is said to be positively chirped when a red-like

wavelength component travels faster, or to be negatively chirped when a blue-like wavelength component travels faster (see **Figures 4** and **5**).

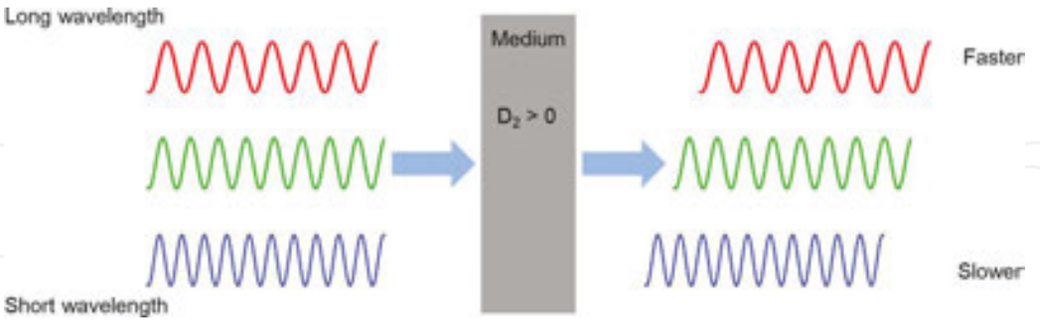


**Figure 4.** Refractive index depending on the wavelength induces the group delay dispersion (GDD). In the positive GDD, the long-wavelength electromagnetic field travels faster than the short-wavelength electromagnetic field in the medium.

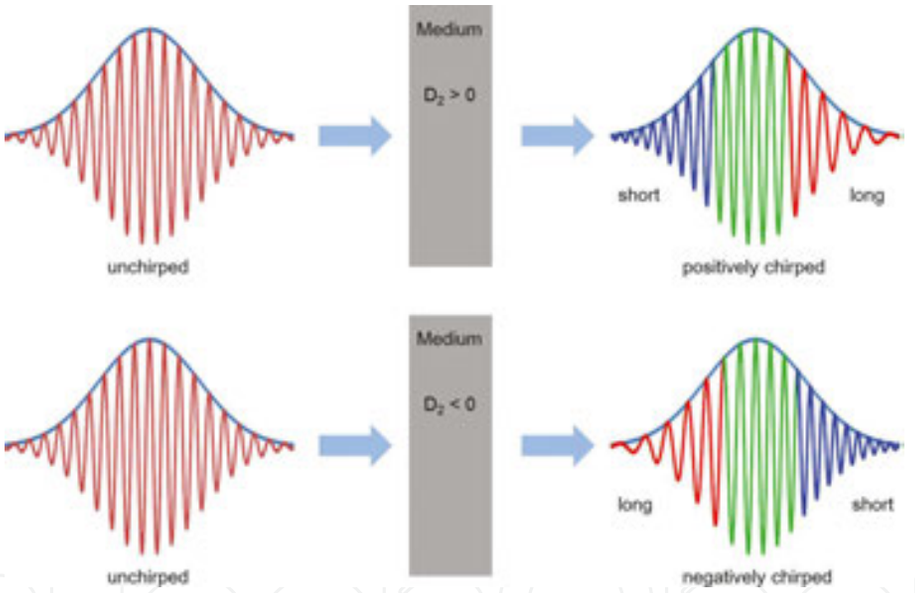


**Figure 5.** Frequency chirping in the laser pulse. In the upper drawing, a short laser pulse experiences the positive chirping, thus the long-wavelength (red) component arrives faster than the short-wavelength (blue) component in the laser pulse. In the lower drawing, a short laser pulse experiences the negative chirping, thus the short-wavelength (blue) component arrives faster than the long-wavelength (red) component. The pulse duration is broadened by the positive or negative chirping.

Higher-order derivatives in the Taylor expansion affect the pulse profile in time as higher-order dispersions. Even-order dispersions are responsible for the symmetric distortion of a laser pulse in time and odd-order dispersions are responsible for the antisymmetric distortion in the laser pulse. The dispersion control and compensation are key techniques to have a transform-limited laser pulse with a given spectrum. Third-order dispersion (TOD) and fourth-order dispersion (FOD) should be considered to be compensated for the generation of transform-limited pulse.

## 2. Amplification of ultrashort laser pulses

The energy of a mode-locked laser pulse with a pulse duration of 1 ps or below typically ranges from $10^{-12}$ to $10^{-10}$ J. The ultrashort laser pulse cannot be directly amplified in amplifiers because of damage issues in optical elements due to the nonlinear effect and the low-energy extraction efficiency. These hurdles were detoured by employing the chirped-pulse amplification (CPA) technique devised by Strickland and Mourou [8]. The key idea of the CPA technique is to temporarily stretch a laser pulse before amplification, to amplify the energy of the stretched pulse, and finally, after energy amplification, to compress the pulse duration to the original level. The CPA technique was well demonstrated in many systems around the world [9], and now it is used for producing the relativistic laser intensity (>$10^{18}$ W/cm$^2$).

The control of pulse duration is usually performed by an optical setup which uses the GDD induced by the grating. The stretched pulse duration ranges from few hundreds of ps to nanosecond (ns). The stretched pulse is amplified in a series of amplifier chain including regenerative and/or multipass amplifiers. The output energy can be estimated from the Frantz-Nodvik equation. In this section, the basic principles for controlling the pulse duration and for amplifying the energy are explained.

### 2.1. Stretching of an ultrashort laser pulse before amplification

The control of pulse duration using the dispersion was first proposed by Treacy [10]. In the proposal, two gratings with a normal separation distance of $b$ are placed in the parallel geometry to induce a negative GDD. The total amount of GDD can be controlled by the separation distance. According to the Treacy's proposal, when a laser pulse passes through an optical setup shown in **Figure 6**, the group delay dispersion (GDD) experienced by a laser pulse is given by

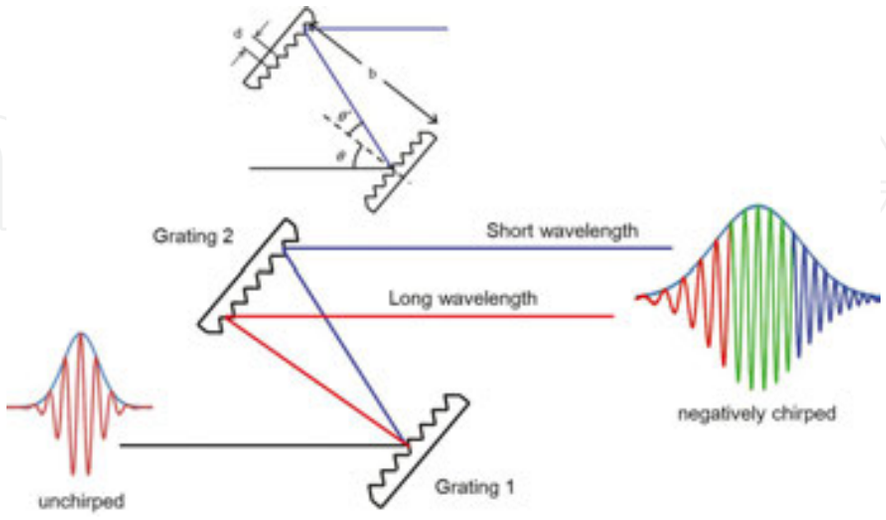


**Figure 6.** Parallel grating pulse stretching scheme. The parallel grating pulse stretcher introduces a negative GDD to the laser pulse.

http://dx.doi.org/10.5772/64526

$$\left.\frac{d^2\phi}{d\omega^2}\right|_{\omega 0} = -\frac{\lambda_0}{2\pi c^2}\left(\frac{\lambda_0}{d}\right)^2 \frac{b}{\cos^3\theta'(\lambda_0)}. \tag{17}$$

Here, $d$ is the groove spacing of grating and $\theta'$ is the diffraction angle. The first-order diffraction is only considered in this case. The diffraction angle is calculated by the grating equation as follows:

$$d\left(\sin\theta' - \sin\theta\right) = \lambda. \tag{18}$$

As shown in Eq. (17), the parallel grating geometry always introduces the negative GDD, and thus the blue-like wavelength component travels faster than the red-like one. The positive GDD can be either introduced by installing a telescope in the parallel grating geometry, which was proposed by Martinez [11]. A telescope is an optical device that induces an angular dispersion. The GDD induced by an angular dispersion is given by

$$\left.\frac{d^2\phi}{d\omega^2}\right|_{\omega 0} \approx -\frac{L_p \cdot \omega_0}{c}\left(\left.\frac{d\alpha}{d\omega}\right|_{\omega 0}\right)^2 \tag{19}$$

with an approximation of $\cos\alpha \gg \sin\alpha$. In the equation, $\alpha$ is the deviation angle at the reference wavelength and $L_p$ is the propagation distance after the surface of an angularly dispersive element. When a laser pulse propagates an optical setup shown in **Figure 7**, the angular dispersion is magnified by a factor of $M$, which is the magnification of a telescope. Then, the GDD induced by the angular dispersion after the propagation of $z'$ is

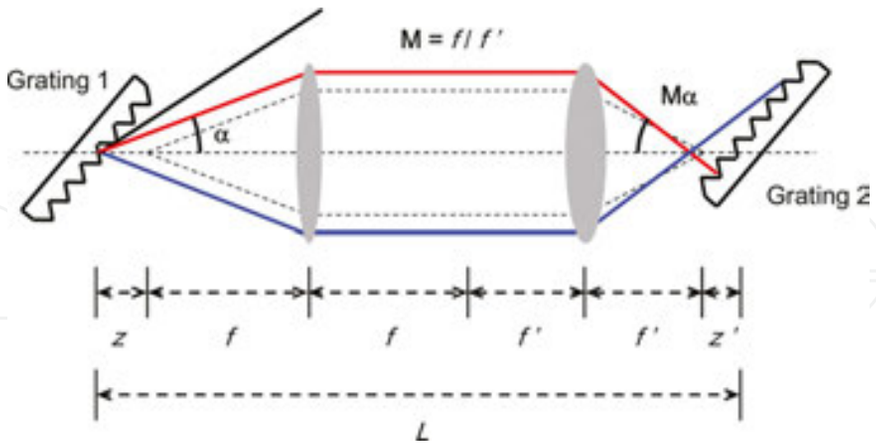


**Figure 7.** GDD control by the grating pair with a telescope inside. The grating pair with the telescope can induce the positive and negative GDD depending on the total length between gratings. The negative GDD is obtained by $L/2 < (f + f')$. The positive GDD is obtained by $L/2 < (f + f')$.

$$\left.\frac{d^2\phi}{d\omega^2}\right|_{\omega 0} = -\frac{\omega_0}{c}\left(\left.\frac{d\alpha}{d\omega}\right|_{\omega 0}\right)^2 z' M^2. \tag{20}$$

As shown in **Figure 7**, the propagation distance $z'$ is given by $L-2(f+f')$ and the magnification by $f/f'$. The positive GDD can be obtained when $L-2(f+f')<0$ or $L/2<(f+f')$. This condition can be met by moving a second grating before the focal point $F'$. In general, the first lens can be placed at a position of $z+f$. Then, an additional GDD, $\frac{d^2\phi}{d\omega^2}\Big|_{\omega 0}=-\frac{\omega_0}{c}\left(\frac{d\theta'}{d\omega}\Big|_{\omega 0}\right)^2 z$, by an angular dispersion after the propagation of $z$ should be added to Eq. (20) to obtain

$$\left.\frac{d^2\phi}{d\omega^2}\right|_{\omega 0}=-\frac{\omega_0}{c}\left(\left.\frac{d\theta'}{d\omega}\right|_{\omega 0}\right)^2\left(z'M^2+z\right). \tag{21}$$

In many cases, a reflecting mirror can be put after the first lens to reduce the cost and space. The positive GDD induced by two grating geometry having a telescope can be compensated for with the parallel grating pair. This is important because the pulse duration stretched by the positive or negative GDD can be recompressed by the negative or positive GDD. This is the principle for stretching and compressing an utrashort laser pulse in the CPA technique. In a common CPA technique, a pulse stretcher introduces a positive GDD to the laser pulse and a pulse compressor introduces a negative GDD. The reason for this is that the material dispersion used in amplifier systems also produces a positive GDD. If a laser pulse has negative GDD by a stretcher, the pulse duration of a pulse is shortened as the pulse propagates in a medium having a positive GDD. This might induce damage on optical elements that the pulse propagates. The other combination that uses a pulse stretcher introducing negative GDD and a pulse compressor introducing positive GDD is also possible. This combination is known as the down-chirped pulse amplification (DCPA) technique and also demonstrated with a grating stretcher and bulk material compressor. Although the DCPA technique works for the energy amplification of an ultrashort laser pulse, the pulse duration of the pulse is somewhat broadened because higher-order dispersions, such as TOD and FOD, induced by media in the laser system remain uncompensated. As mentioned earlier, third-order dispersion (TOD), and fourth-order dispersion (FOD) should be corrected or optimized to obtain a nearly transform-limited pulse duration through the pulse compressor.

The misalignment in the parallelism of a grating induces an additional angular dispersion in the spatial domain. This is known as the spatial chirping. The spatial chirping can easily be examined by monitoring the intensity distribution of a focal spot. If there is the spatial chirping in the laser beam profile, a focal spot is elongated along the chirping direction. Sometimes, the elongation by the spatial chirping is confused with astigmatism in the beam. However, the spatial chirping can be discriminated by the through-the-focus image because the elongation by the spatial chirping is not rotated by 90 degrees while the elongation by astigmatism can be rotated.

### 2.2. Rate equation

When a laser pulse passes through an amplification medium, the pulse obtains energy gain from the medium. The energy gain comes from a stored energy in the medium which is provided by an external power source. Absorption by the transition between electronic energy

http://dx.doi.org/10.5772/64526

levels is used to store an external energy. Electrons at a lower energy level are excited to a higher energy level through the pumping process. When an electromagnetic wave (photon) with a specific wavelength defined by the atomic energy transition is radiated to an excited atom, the atom emits the same electromagnetic wave (photon) as the incoming one. This means that an incoming electromagnetic wave is amplified in intensity. This dynamics can be described by the rate equation. In order to describe the situation mathematically, let us consider a four-energy-level system shown in **Figure 8**.

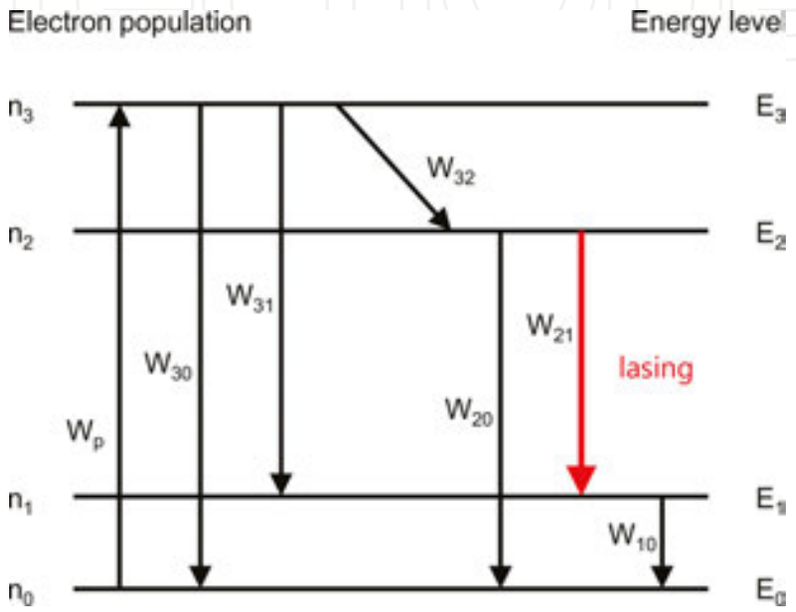


**Figure 8.** Diagram for energy levels, level transition rate, and the number of electrons at the energy level. In the four-level system, the storage of external energy is accomplished by the absorption due to the electronic transition from level 0 to level 3, and the lasing or energy gain is obtained by the electronic transition from level 2 to level 1.

In a four-level system shown in **Figure 8**, electrons at the lowest energy level 0 are excited to level 3 by the pumping process. The changing rate for the excited electron population increases by the electron population at level 0 and the pumping rate $W_p$. In a short time, electrons at level 3 lose their energy and decay into level 2 with a transition probability $W_{32}$. Electrons at level 3 also decay into level 1 and 0 with probabilities $W_{31}$ and $W_{30}$. The changing rate for electron population at level 2 increases with the number of electrons at level 3 and the transition probability $W_{32}$, and it decreases with the number of electrons at level 2 and transition probabilities $W_{21}$ and $W_{20}$ to level 1 and level 0, respectively. The main lasing action or energy gain happens with the transition from level 2 to level 1. Under this circumstance, the rate equations for electrons at each level can be expressed as

$$\frac{dn_3}{dt} = W_p n_0 - W_{32} n_3 - W_{31} n_3 - W_{30} n_3 , \tag{22-1}$$

$$\frac{dn_2}{dt} = W_{32} n_3 - W_{21} n_2 - W_{20} n_2 , \tag{22-2}$$

$$\frac{dn_1}{dt} = W_{31}n_3 + W_{21}n_2 - W_{10}n_1 , \tag{22-3}$$

$$\frac{dn_0}{dt} = -W_p n_0 + W_{30}n_3 + W_{20}n_2 + W_{10}n_1 . \tag{22-4}$$

Although rate equations for level 1 and level 0 are not explained here, those can be easily derived from **Figure 8**. In the four-level system, it is assumed that electron populations at levels 1 and 3 are very small because of the rapid transition to other levels, i.e., $n_2$, $n_0 \gg n_3$, $n_1$. The total number, $n$, of electrons is determined by the sum of electron numbers at levels 0 and 2, i.e., $n = n_2 + n_0$. In the steady-state condition, the change of electron populations at levels 3 and 2 are very small as well; so, we assume $\frac{dn_3}{dt} = \frac{dn_2}{dt} \approx 0$. From Eqs. (22-1) and (22-2), we obtain

$$\frac{n_2}{n_0} = \frac{W_p}{(W_{21} + W_{20})} \frac{W_{32}}{(W_{32} + W_{31} + W_{30})} . \tag{23}$$

At level 2, the approximation of $W_{21} \gg W_{20}$ is valid because the lasing action or gain is dominant. And, electron transition from level 3 to level 2 is most dominant to the other transition and thus $W_{32} \gg W_{31}$, $W_{30}$. Under these conditions, Eq. (23) reduces to

$$\frac{n_2}{n_0} = \frac{W_p}{W_{21}} \tag{24}$$

According to Eq. (24), a laser pulse can have energy gain when $n_2 > n_0$. The population inversion happens when the difference, $\Delta n = n_2 - n_0$, in electron numbers at levels 2 and 0 is positive. Under the heavily pumping condition, most electrons exist in level 2, and the number of electrons ($n_2$) at level 2 approximately equals $n_0$. The population inversion is given by

$$\Delta n = n_2 \left(1 - \frac{W_{21}}{W_p}\right) \approx \frac{n}{1 + W_{21}/W_p} . \tag{25}$$

By using the relation of $W_{21}/W_p = I(z)/I_{sat}$, Eq. (25) becomes $\Delta n \approx n/(1 + I/I_{sat})$. When a low-intensity laser pulse propagates in the gain medium, the intensity growing rate is linear with the product of propagation distance and population inversion as shown below:

$$\frac{dI(z)}{dz} = I(z)\sigma_{21}\Delta n . \tag{26}$$

Here, $\sigma_{21}$ is the emission cross section. By inserting the relation of $\Delta n \approx n/(1 + I/I_{sat})$ into Eq. (26), the growing rate for the intensity becomes

$$\frac{dI(z)}{dz} = I(z)\frac{\sigma_{21}n}{1+I(z)/I_{sat}} \text{ or } \frac{dI(z)}{dz} = g(z)I(z). \tag{27}$$

In Eq. (27), the gain $g(z)$ is defined by $g_0/(1 + I(z)/I_{sat})$ and $g_0$ is defined by $\sigma_{21}n$. When the intensity of a laser pulse is small enough, the intensity exponentially grows with $I_0 \exp(\int g(z)dz)$. The gain, $\exp(\int g(z)dz)$, at a small input intensity is known as the small signal gain. As the intensity becomes stronger, the growing rate for the intensity starts to be lowered and the intensity linearly grows with $gL$ in the saturation regime, where $L$ is the medium length.

### 2.3. Energy amplification

The small signal gain describes how much intensity or energy can be achieved with a given small input intensity. The small intensity means an intensity level that does not affect the population inversion. In this subsection, we will describe the energy amplification in an amplifier system. A single-pass energy gain can be measured by putting a detector before and after the amplification medium during the energy measurement experiment. The small signal and single-pass gain, $G_0$, at the first pass is given by $\exp(\int g(z)dz)$ or simply by

$$G_0 = \exp(g_0 L). \tag{28}$$

Here, $g_0$ is the measured gain coefficient and $L$ is the medium length. Using the Frantz-Nodvik equation [12], the output energy of a laser pulse at the $i$th round trip in the amplifier can be expressed by

$$F_i = F_{sat} \ln\left[1 + G_i\left\{\exp\left(\frac{F_{i-1}}{F_{sat}}\right) - 1\right\}\right]. \tag{29}$$

Here, $F$ means the fluence of a laser pulse defined by $\int_{-\infty}^{\infty} I(z, t)dt$ and the subscripts ($i$ and $i - 1$) mean the $i$th and ($i - 1$)th round trips. $F_{sat}$ is the saturation fluence. In a multipass amplifier system, an amplified laser pulse is reinjected into the amplifier medium. Thus, the gain decreases as the input intensity increases. The reduced gain at the $i$th round trip can be calculated from the gain and the fluence at the ($i - 1$)th round trip as follows:

$$G_i = \left\{1 - \left(1 - \frac{1}{G_{i-1}}\right)\exp\left(-\frac{F_{i-1}}{F_{sat}}\right)\right\}^{-1}. \tag{30}$$

**Figure 9** shows the amplified output energy as a function of the round trip in a multipass amplifier. In the calculation, the Ti:sapphire crystal is assumed as an amplifier medium. The saturation fluence of the Ti:sapphire crystal is 1.2 J/cm$^2$ and the small signal gain of 3.5 is assumed. The energy exponentially increases in the first few round trips, but the energy

linearly increases as the energy becomes comparable to the saturation energy of the amplifier medium. Finally, the output energy is saturated at a certain energy level which is close to the saturation fluence.

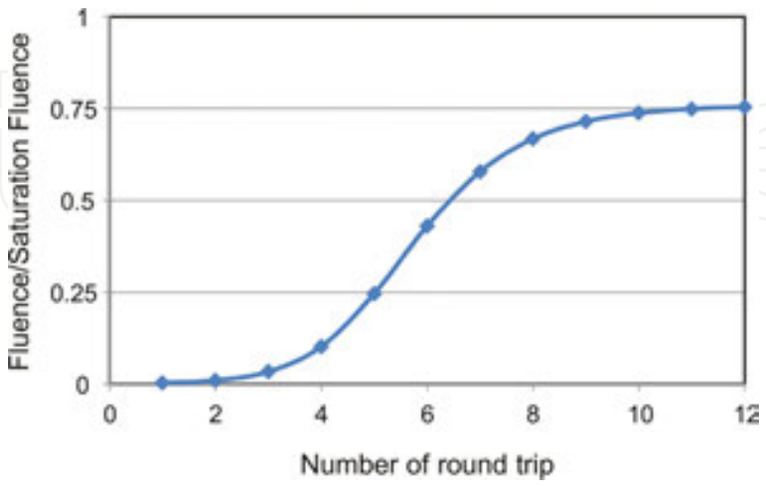


**Figure 9.** Fluence of the laser pulse with respect to the number of round trip. The input fluence was 1 mJ and the small signal gain was assumed to be 3.5.

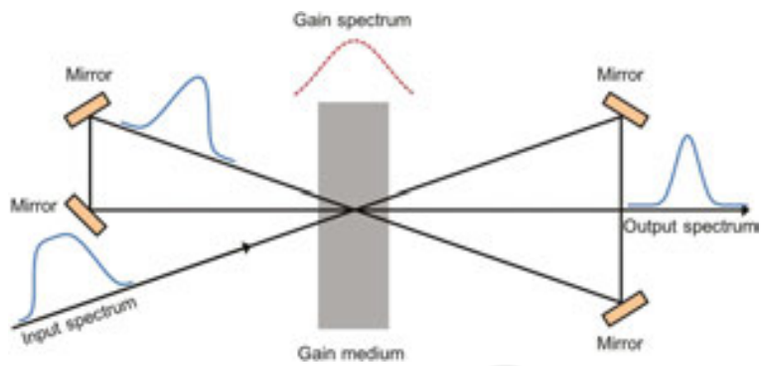


**Figure 10.** Diagram explaining the gain narrowing effect. The origin of the gain narrowing effect is an un-equal gain at a different wavelengths. The wavelength component at a higher gain grows faster than that at a lower gain. The gain narrowing effect broadens the pulse duration of the compressed pulse.

A series of amplifier system including a regenerative amplifier and multiple-stage amplifiers are used for energy amplification. The final output energy ranges from a couple of J to ~100 J, depending on the peak power level. The pulse energy should be amplified by a factor of ~$10^{12}$ while keeping the pulse characteristics the same. This is not easy because of the gain narrowing effect induced by the different gains at different wavelengths. The gain narrowing phenomenon happens because a wavelength component located at a higher gain becomes stronger than a wavelength component at a lower gain as shown in **Figure 10**. The gain narrowing broadens the pulse duration of a compressed pulse. Several techniques, such as input intensity modulation, wavelength mismatch between the input and gain spectrum, gain saturation, and so on, have been developed to minimize the gain narrowing effect.

The amplified spontaneous emission (ASE) occurred in a large size gain crystal reduces an overall gain and deteriorates the spatial profile of a laser pulse as shown in **Figure 11**. A spontaneous emission traveling in the transverse direction of the gain medium has energy gain before the laser pulse arrives. When the gain and the size of gain medium are small, the ASE is negligible during the amplification process. However, as the size of gain medium is large enough with a considerable gain, the ASE becomes significant. In order to reduce the ASE, the gain medium is enclosed by the light-absorption cooling liquid having a refractive index similar to the gain medium. With the cooling liquid, the spontaneous emission transmits the boundary between the gain medium and cooling liquid, and scattered in the mount. Thus, the ASE reflected from the boundary can be suppressed. Sometimes, the spontaneous emission has enough energy gain even in a single transverse pass. In this case, a delayed pumping scheme can be useful to reduce the ASE.

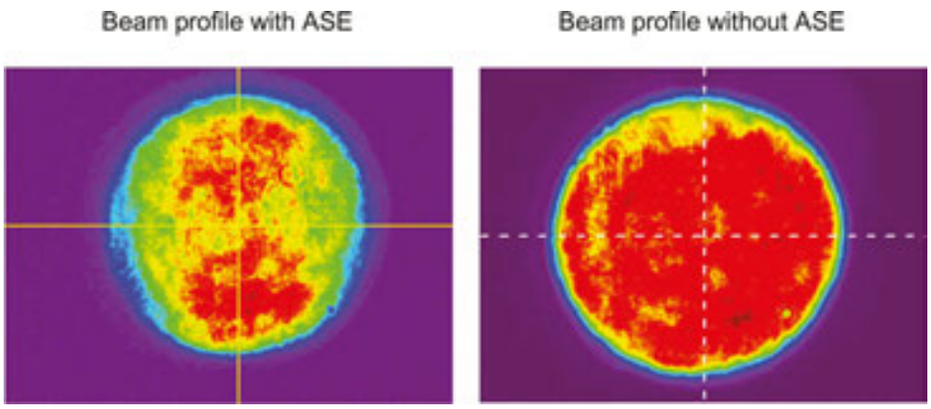


**Figure 11.** Laser beam profile with and without the amplified spontaneous emission (ASE). The ASE reduces energy gain and deteriorates beam profile.

Since the demonstration of laser in 1960, the laser technology has continuously advanced to build petawatt (PW) laser systems. In 1999, the first CPA PW laser has been demonstrated using a Ti:sapphire/Nd:glass hybrid system [13]. Almost a decade later, 30 fs 1 PW laser operating at 0.1 Hz repetition rate was developed [14] and more recently an amplifier for 5 PW laser system has been successfully demonstrated [15]. Now, fs and 10 PW laser systems are under construction through the European Extreme Light Infrastructure (ELI) program.

## 3. Focusing ultrashort laser pulses

An amplified and compressed laser pulse is focused on solid or gas target for laser-matter interaction studies. Concave mirrors are generally used and the intensity reaches at a relativistic level, $>10^{18}$ W/cm$^2$. The size of a focal spot is proportional to the focal length of a mirror and a shorter focal length is preferable to reach a higher intensity. Thus, one particular research interest is to tightly focus a laser pulse to reach an unprecedented intensity level. The paraxial approximation, which is commonly used in calculating focal spots under high *f*-number

conditions, becomes invalid under tight focusing (low *f*-number) conditions. Intensities of a focal spot that have other polarization components different from an incident polarization are assumed to be negligible in the paraxial approximation. However, under tight focusing conditions, intensities at different polarizations increase and modify the overall intensity distribution of a focused laser pulse.

The intensity distributions of all polarization components of a focal spot formed under a tight focusing condition can be calculated by vector diffraction integrals developed by Stratton and Chu [16]. Recently, the intensity distributions of a focused fs high-power laser pulse under a tight focusing condition were intensively examined [17]. In this section, the intensity distributions of a tightly focused laser spot are described. The accurate assessment of the peak power and information on the intensity distribution are beneficial in simulating and predicting the motion of charged particles under a super-strong laser pulse that is provided by a tight focusing scheme.

### 3.1. Modeling of focusing scheme with low *f*-number parabolic mirror

The parabolic mirror is used as a focusing mirror because of its quadratic surface profile. A linearly polarized (x-polarized) laser pulse having an electric field distribution, $E_{\mathrm{inc}}(\theta_S, \phi_S)$, is incident on a parabolic mirror along the negative *z*-direction (**Figure 12**). By using Sttraton and Chu's vector diffraction integrals, the electric fields at all polarization components can be expressed as follows:

$$E_x\left(x_P, y_P, z_P\right) \sim \int_{\theta m}^{\pi}\int_0^{2\pi} d\theta_S d\phi_S E_{inc}\left(\theta_S, \phi_S\right) \exp\left\{-ik\varphi\left(x_P, y_P, z_P, \theta_S, \phi_S\right)\right\} \frac{2f\sin\theta_S}{\left(1-\cos\theta_S\right)} \times\left\{1-\frac{\sin\theta_S\cos\phi_S}{1-\cos\theta_S}\left(1-\frac{1-\cos\theta_S}{i2kf}\right)\frac{2f\sin\theta_S\cos\phi_S - x_P\left(1-\cos\theta_S\right)}{2f}\right\}, \tag{31-1}$$

$$E_y\left(x_P, y_P, z_P\right) \sim \int_{\theta m}^{\pi}\int_0^{2\pi} d\theta_S d\phi_S E_{inc}\left(\theta_S, \phi_S\right) \exp\left\{-i\varphi\left(x_P, y_P, z_P, \theta_S, \phi_S\right)\right\} \frac{2f\sin\theta_S}{\left(1-\cos\theta_S\right)^2} \times\left\{\sin\theta_S\cos\phi_S\left(1-\frac{1-\cos\theta_S}{i2kf}\right)\frac{2f\sin\theta_S\sin\phi_S - y_P\left(1-\cos\theta_S\right)}{2f}\right\}, \tag{31-2}$$

$$E_z\left(x_P, y_P, z_P\right) \sim \int_{\theta m}^{\pi}\int_0^{2\pi} d\theta_S d\phi_S E_{inc}\left(\theta_S, \phi_S\right) \exp\left\{-i\varphi\left(x_P, y_P, z_P, \theta_S, \phi_S\right)\right\} \frac{2f\sin\theta_S}{\left(1-\cos\theta_S\right)^2} \times\sin\theta_S\cos\phi_S\left\{1-\left(1-\frac{1-\cos\theta_S}{i2kf}\right)\frac{2f\cos\theta_S - z_P\left(1-\cos\theta_S\right)}{2f}\right\}, \tag{31-3}$$

and

$$\varphi\left(x_P, y_P, z_P, \theta_S, \phi_S\right) = k\left(z_P\cos\theta_S + x_P\sin\theta_S\cos\phi_S + y_P\sin\theta_S\sin\phi_S\right). \tag{31-4}$$

http://dx.doi.org/10.5772/64526

Here, $f$ is the focal length of a mirror. $x_P$, $y_P$, and $z_P$ represent positions at vicinities of the focal point. $\theta_S$ is the polar angle measured from the positive $z$-axis and $\phi_S$ is the rotational angle measured from the positive $x$-axis. The minimum angle, $\theta_{\min}$, determines the $f$-number of the mirror. The distance between the source (s) and observation (p) points is expressed as $2f/(1 - \cos\theta_S)$ for the intensity of a laser spot and as $2f/(1 - \cos\theta_S) - \rho_P\{\cos\theta_S \cos\theta_P + \sin\theta_S \sin\theta_P \cos(\phi_S - \phi_P)\}$ for the phase of the spot.

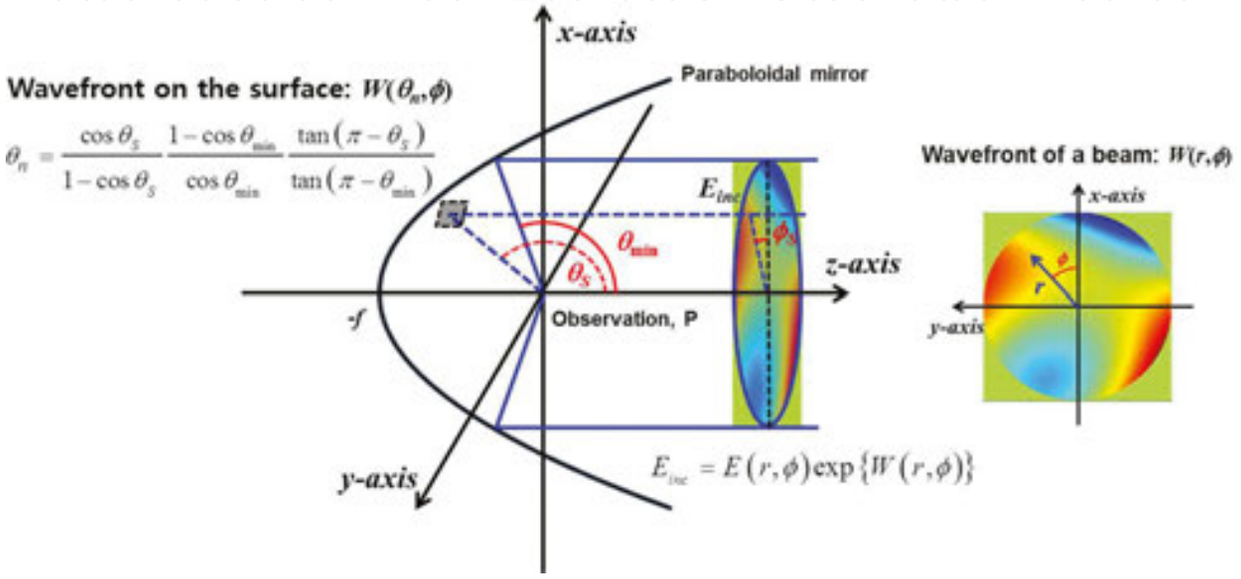


**Figure 12.** On-axis focusing scheme for an aberrated laser beam with a low $f$-number parabolic mirror.

The wavefront aberration of a laser pulse is one of the factors that determines the intensity distribution of a focal spot. The wavefront aberration is the phase delay function across the laser beam and included in the incident electromagnetic field of a laser pulse as follows:

$$E_{inc}(\theta_S,\phi_S) = E_0(\theta_S,\phi_S)\exp\{ikW_{inc}(\theta_n,\phi_S)\}. \tag{32}$$

Here, $\theta_n$ can be interpreted as a normalized radius defined by $(\pi - \theta_S)/(\pi - \theta_{\min})$. The wavefront aberration is expressed by the Zernike polynomials as $W_{inc}(\theta, \phi) = \sum_{u,v} c_u^v Z_u^v(\theta_n, \phi_S)$. In this case, $c_u^v$ means the Zernike coefficient, and $Z_u^v(\theta_n, \phi_S)$ is the Zernike polynomial for the $u$th radial and the $v$th azimuthal orders, respectively. The entire phase function on the mirror surface is modified as $k(z_P \cos\theta_S + x_P \sin\theta_S \cos\phi_S + y_P \sin\theta_S \sin\phi_S) + kW_{inc}(\theta_n, \phi_S)$. For a high $f$-number case, $\theta_S$ and $\theta_n$ are almost the same, and the wavefront, $W_S(\theta_n, \phi_S)$, on the mirror surface is almost equivalent to $W_{\text{inc}}(\theta_S, \phi_S)$. However, as the $f$-number of a parabolic mirror decreases, the wavefront on the mirror surface becomes different from the wavefront of an incident wave. In this case, the normalized radius, $\theta_n$, on the mirror surface is modified and given by

$$\theta_n = \frac{\cos\theta_S}{1-\cos\theta_S}\frac{1-\cos\theta_{\min}}{\cos\theta_{\min}}\frac{\tan(\pi-\theta_S)}{\tan(\pi-\theta_{\min})}. \tag{33}$$

The change in wavefront aberration due to the polarization rotation after reflection from a mirror surface should be considered for the effect of polarization. Thus, after reflection from a parabolic mirror, the normal vector to the wavefront surface is expressed by $2\hat{n}(\vec{S}\cdot\hat{n})-\vec{S}$ as shown below:

$$2\hat{n}\left(\vec{S}\cdot\hat{n}\right)-\vec{S} = \left(\hat{x}\sin\theta_S\cos\phi_S + \hat{y}\sin\theta_S\sin\phi_S - \hat{z}\cos\theta_S\right)W_S\left(\theta_n,\phi_S\right) \tag{34}$$

Expressions for normal vectors on a parabolic mirror surface which are given by

$$n_x = \frac{\sin\theta_S\cos\phi_S}{\left[2\left(1-\cos\theta_S\right)\right]^{1/2}},\ n_z = \left(\frac{1-\cos\theta_S}{2}\right)^{1/2},\ \text{and}\ n_y = \frac{\sin\theta_S\sin\phi_S}{\left[2\left(1-\cos\theta_S\right)\right]^{1/2}} \tag{35}$$

are used in the calculation of Eq. (34). Finally, the wavefront component that propagates to the $\rho$-direction contributes to the formation of an intensity distribution near the focal plane and is given by

$$\left[2\hat{n}\left(\vec{S}\cdot\hat{n}\right)-\vec{S}\right]\cdot\vec{k}_\rho = \frac{2\pi}{\lambda}W_S\left(\theta_n,\phi_S\right)\left\{\sin^2\theta_S\cos 2\phi_S + \cos^2\theta_S\right\} \tag{36}$$

with $\hat{\rho} = \hat{x}\sin\theta_S\cos\phi_S - \hat{y}\sin\theta_S\sin\phi_S - \hat{z}\cos\theta_S$. But, as expected in Eq. (36), the contribution by the $\{\cdot\}$ term is not significant when $\sin^2\theta_S\cos 2\phi_S \ll \cos^2\theta_S$.

### 3.2. Coherent superposition of monochromatic fields for femtosecond focal spot

A femtosecond laser pulse typically has a broad spectrum of several tens of nm, thus the effect of broad spectrum of a femtosecond laser pulse on the focal spot should be considered in order to accurately describe the focal spot of a femtosecond laser pulse. The spatial and temporal profiles of a femtosecond focal spot can be calculated by the superposition of monochromatic electric fields near the focal point. The resultant electric fields for a femtosecond focal spot are expressed with spectral amplitude and phase as below (see **Figure 13**):

$$\begin{aligned} E_{x,y,z}\left(x_P,y_P,z_P\right) = {} & R_{\lambda 1}\exp\left(i\alpha_{\lambda 1}\right)E_{x,y,z}\left(\lambda_1 : x_P,y_P,z_P\right) + R_{\lambda 2}\exp\left(i\alpha_{\lambda 2}\right)E_{x,y,z}\left(\lambda_2 : x_P,y_P,z_P\right) + \\ & \cdots + R_{\lambda n}\exp\left(i\alpha_{\lambda n}\right)E_{x,y,z}\left(\lambda_n : x_P,y_P,z_P\right) \end{aligned}. \tag{37}$$

Here, $R_\lambda$ defined by $\sqrt{I_\lambda / I_{\lambda,\max}}$ and $\alpha_\lambda$ are the relative amplitude and the spectral phase at a given wavelength, respectively. The subscripts ($x$, $y$, $z$) represent the polarization directions and $E_{x,y,z}(\lambda_n : x_P, y_P, z_P)$ induces the monochromatic electric field. Contrary to the monochromatic case, a different field oscillation period at a different wavelength induces a phase mismatch

http://dx.doi.org/10.5772/64526

among waves at different wavelengths and reduces the intensity quickly as the observation position moves away from the origin of the focal plane. The intensity distribution along the propagation direction can be interpreted as the temporal profile of a femtosecond focal spot. Thus, the resultant electric fields, $E_{x,y,z}(x_P, y_P, z_P)$, provide the spatial and temporal (spatiotemporal) intensity distributions of a laser focal spot. The resultant electric fields are numerically calculated. In the calculation, the spectrum is sliced into $n$ components. The monochromatic electric field distributions at all polarization components are obtained from Eqs. (31-1)–(31-4). The relative amplitude ratio and the spectral phase are obtained by the measurement of a laser pulse. After calculating the resultant electric fields, the final intensity distributions at all polarization components become

$$I_{x,y,z}(x_P, y_P, z_P) \propto \left| E_{x,y,z}(x_P, y_P, z_P) \right|^2. \tag{38}$$

This approach provides information on intensity distribution at all polarization components both in temporal and spatial domains and it is also valid under high $f$-number focusing conditions as well. The sum of all polarization components given by $I_x(x, y, z) + I_y(x, y, z) + I_z(x, y, z)$ is the intensity distribution measured by an image-sensing device.

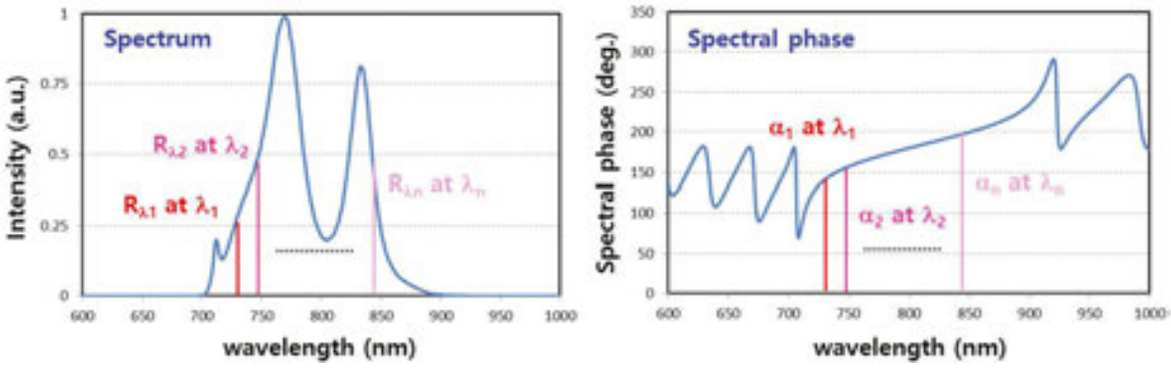


**Figure 13.** Spectrum and spectral phase for calculating the femtosecond focal spot.

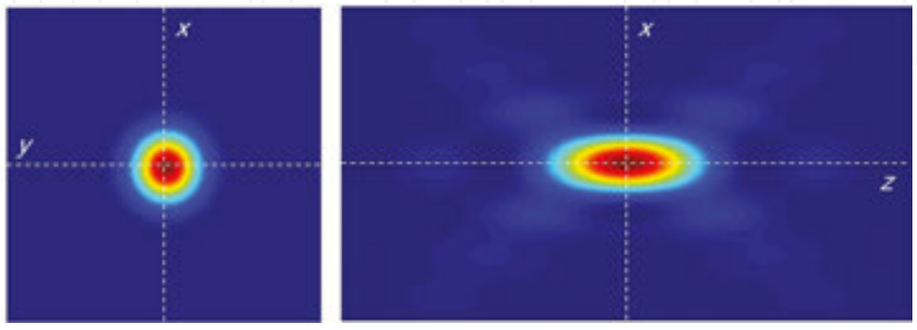


**Figure 14.** Three-dimensional intensity distribution of the continuous wave and spatially uniform laser beam under loose focusing condition. The x-polarized beam is assumed and the laser beam propagates along the −z direction. Under the far-field approximation, the x-polarization component is only considered to calculate the intensity distribution.

### 3.3. Intensity distribution in the focal plane and its vicinity

Under the loose focusing condition ($f/\# >> 1$), the intensity distribution having the same polarization as an incoming laser pulse is only considered, and other polarization components ($I_y(x, y, z)$ and $I_z(x, y, z)$) are ignored. In this case, the far-field approximation is applied and the Fourier transform of an incoming electric field, which is derived from the scalar diffraction integral, is widely used to obtain the intensity distribution of a focal spot. **Figure 14** shows the typical intensity distributions in the $x$-$y$ plane and the $x$-$z$ plane.

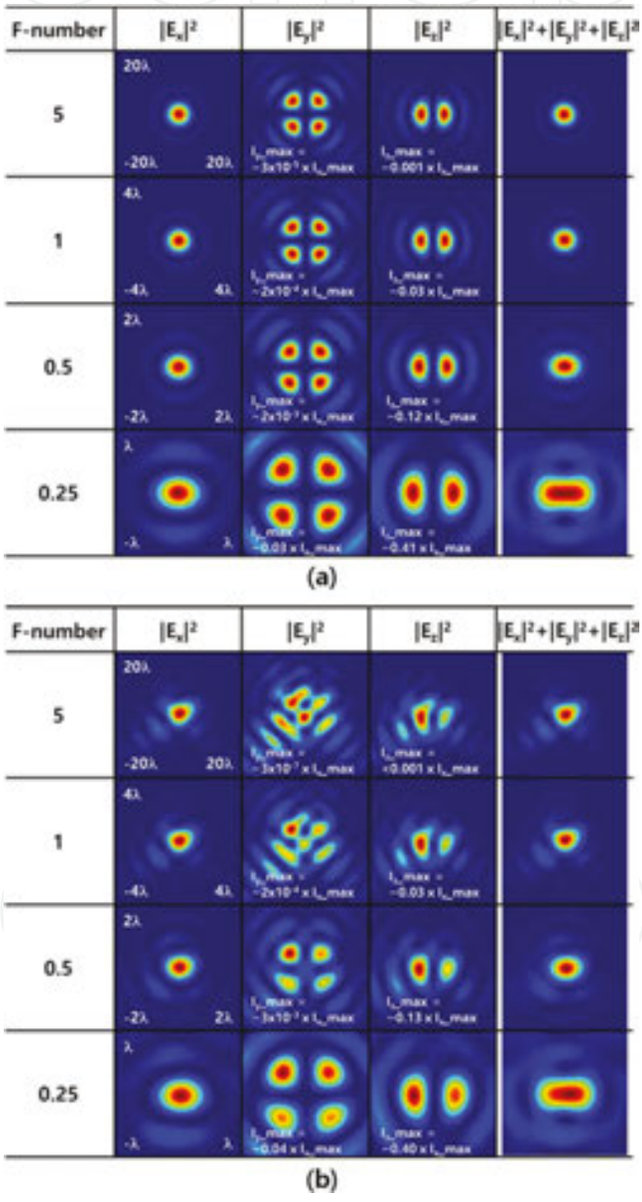


**Figure 15.** The change in intensity distributions as the $f$-number decreases. The intensity distributions for a continuous wave and uniform laser beam are calculated in the focal plane. (a) The ideal uniform laser beam profile without wavefront aberration is assumed as an input. (b) The uniform beam profile with wavefront aberration is assumed as an input.

Intensities having other polarizations different from an incoming laser pulse increase under the tight focusing condition. Typical aspects under tight focusing conditions are the increase in the intensity of a longitudinal polarization component and the elongation of a focal spot along the polarization direction. **Figure 15(a)** shows the change in the intensity distribution when the *f*-number of a parabolic mirror decreases from 5 to 0.25. The peak intensity of a longitudinal component, $I_z$, increases up to 41% of that of $I_x$ under *f*/0.25 condition. But, compared to the x-polarization component, the peak intensity of the y-polarized component, $I_y$, is still negligible. Because of the increase of intensity in the longitudinal component and the deformation of x-polarized intensity, the resultant intensity is elongated in the polarization direction as shown in **Figure 15(a)**.

**Figure 15(b)** shows the change of a focal spot for an aberrated laser pulse as the *f*-number decreases. A small amount of wavefront aberration ($c_2^{-2}$ = 0.07 μm, $c_3^{-3}$ = 0.05 μm, $c_3^{-1}$ = 0.04 μm, and $c_3^{1}$ = 0.02 μm) was introduced to the laser pulse to investigate the effect of wavefront aberration on the focal spot. The figure shows how the focal spot of an aberrated laser pulse is influenced by the focusing condition. Under a high *f*-number condition (*f*/5), the focal spot of an aberrated laser pulse is determined by the spatial characteristics of the laser pulse, such as wavefront aberration and spatial profile. The shape of the focal spot was almost same as that obtained with the Fourier transform method because the focusing condition and the amount of wavefront aberration did not violate the far-field and thin-lens approximations. Instead, under lower *f*-number conditions, focal spots are also influenced by the vectorial properties, resulting in the elongation along the polarization direction. With a given amount of wavefront aberration, the peak intensity of a longitudinal component, $I_z$, increases up to 40% of that of $I_x$ under *f*/0.25 condition. Further calculation with a higher amount of wavefront aberration ($c_2^{2}$ = $c_2^{-2}$ = $c_3^{-1}$ = 0.15 μm) shows that intensity distribution under *f*/0.5 focusing condition was still different from the intensity distribution obtained with the Fourier transform method.

**Figure 16** shows spatiotemporal intensity distributions of femtosecond focal spots for an aberrated laser pulse under two different focusing conditions (*f*/3 and *f*/0.5). The Zernike coefficient that are used again include $c_2^{-2}$ = 0.07 μm, $c_3^{-3}$ = 0.05 μm, $c_3^{-1}$ = 0.04 μm, and $c_3^{1}$ = 0.02 μm. In the figure, the intensity distributions in the *x*-*y* plane provide information on spatial profiles of a femtosecond focal spot, and the intensity distributions in the *x*-*z* plane provide information on temporal profiles. By assuming a 12 fs, 10 PW, uniformly circular, and aberrated laser pulse as an input, peak intensities for x-polarized component increases up to ~$8.8 \times 10^{22}$ W/cm$^2$ for *f*/3 and ~ $2.5 \times 10^{24}$ W/cm$^2$ for *f*/0.5, respectively. Under same conditions, peak intensities for longitudinal component rapidly increase to ~$3.1 \times 10^{20}$ W/cm$^2$ and ~$2.4 \times 10^{23}$ W/cm$^2$. These intensities along the *z*-direction should be taken into account to better describe the motion of charged particles under an extremely strong EM field that is formed by tightly focusing a femtosecond high-power laser pulse.

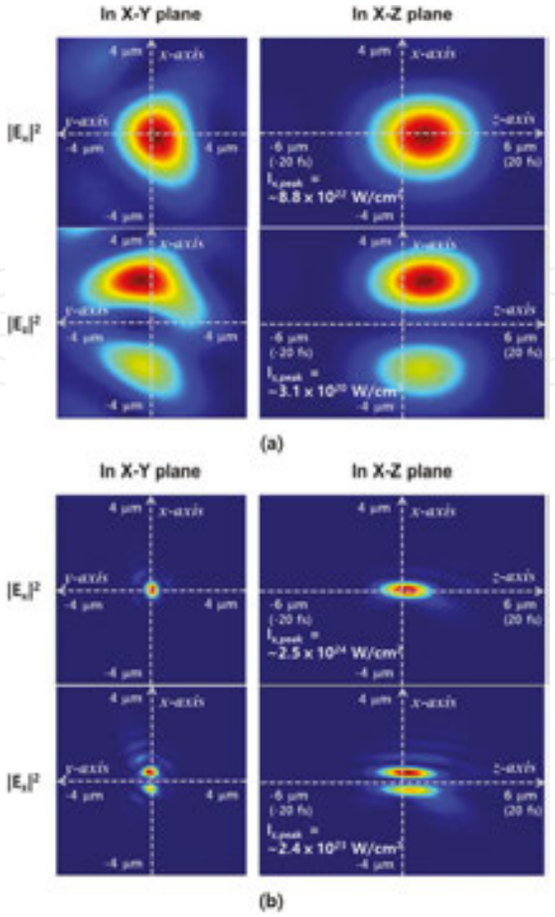


**Figure 16.** The spatiotemporal intensity distributions of a focal spot with (a) an *f*/3 parabolic mirror and (b) an *f*/0.5 parabolic mirror. The peak intensities of $I_x$ reach ~8.8 × $10^{22}$ W/cm$^2$ and ~2.5 × $10^{24}$ W/cm$^2$ for *f*/3 and *f*/0.5 focusing conditions, respectively. The transverse intensity distribution is expressed in the *x*-*y* plane and the longitudinal intensity distribution is expressed in the *x*-*z* plane.

## 4. Interaction of an intense laser pulse with plasma

Under a strong electromagnetic field, the motion of an electron is governed by the Lorentz force as follows:

$$\frac{d\left(\gamma m_0 \vec{v}\right)}{dt} = -e\vec{E} - e\left(\frac{\vec{v}}{c} \times \vec{B}\right). \tag{39}$$

Here, $m_0$ is the electron rest mass, $c$ is the speed of light, and $\gamma$ is the Lorentz factor. When the electromagnetic field is not strong enough, the $\frac{\vec{v}}{c} \times \vec{B}$ term on the right-hand side is much less than the first term on the right-hand side and negligible. In this case, the Lorentz force is reduced to $d(m\vec{v})/dt = -e\vec{E}$. By assuming the sine wave for the electric field and replacing the time derivative by $-i\omega$, then the speed of an electron is

http://dx.doi.org/10.5772/64526

$$v = \frac{e}{m\omega} E(t). \tag{40}$$

The maximum speed of an electron is given by $v_{max} = eE_0/m\omega$. By comparing the maximum speed of an electron and the speed of light, we define $\beta = v/c$. In the nonrelativisitic approach, we can consider $\beta = 1$ as a reference. Then, the intensity required for an electron to have the speed of light $c$ is given by

$$I = \frac{\varepsilon_0 c}{2}\left(\frac{2\pi mc^2}{\lambda e}\right)^2. \tag{41}$$

The intensity for the speed of light is ~ 2.14 × $10^{18}$ W/cm$^2$ for the 0.8 μm wavelength. In the nonrelativistic approach, the intensity of $10^{18}$ W/cm$^2$ is roughly estimated for electrons to have a quiver motion in which the speed is close to the speed of light. The intensity of $10^{18}$ W/cm$^2$ is known as the relativistic intensity for the electromagnetic field.

As shown in the previous section, the relativistic intensity is easily obtained by focusing a femtosecond high-power laser pulse. The femtosecond focal spot has a finite extent in the temporal and spatial domains. Let us expand the electric field of a high-power laser pulse in the Taylor series at a position of $x_0$, then we obtain

$$E_x(r) \simeq E_x(r)\big|_{r=x0}\cos(kz-\omega t) + x\left.\frac{\partial E_x(r)}{\partial x}\right|_{r=x0}\cos(kz-\omega t) + \cdots \tag{42}$$

By inserting the first term on the right-hand side in Eq. (42) into the first term in Eq. (39) and solving the equation, the velocity and the position of electron are given by

$$v_x = -\frac{eE_x(r)\big|_{r=x0}}{m\omega}\sin(kz-\omega t) \text{ and } x = -\frac{eE_x(r)\big|_{r=x0}}{m\omega^2}\cos(kz-\omega t). \tag{43}$$

In order to see the effect of the intensity (or field) gradient of a focused intensity, let us put the expression of $x$ in Eq. (43) into Eq. (42) and consider the Lorentz force again. Then, we obtain

$$m\frac{d}{dt}v_x = -\frac{e^2}{2m\omega^2}\left.\frac{\partial E_x^2(r)}{\partial x}\right|_{r=x0}\cos^2(kz-\omega t). \tag{44}$$

By taking the cycle average of the force, Eq. (44) becomes

$$m\frac{d}{dt}v_x = -\frac{e^2}{4m\omega^2}\left.\frac{\partial E_x^2(r)}{\partial x}\right|_{r=x0}. \tag{45}$$

Eq. (45) means that an electron can be pushed by the intensity or the field gradient. The force due to the intensity gradient is known as the ponderomotive force.

When a high-power laser pulse is focused in a gas target, the target immediately turns into the plasma medium. Electrons in the plasma medium feel the ponderomotive force by the laser pulse in temporal and spatial domains, and those are pushed by a focused laser field and separated from the background ions. The separation of electrons from background ions induces a strong electric field by the space charge effect. The periodic motion of oscillation for electrons occurs around heavy ions as the laser pulse propagates. The resultant pattern of alternating positive and negative charges is known as the plasma wave or laser wake. The laser wake field supports a very strong longitudinal electric field of 1 GeV/cm. Some of returning electrons can be captured into the laser wake and accelerated by the laser wake field up to GeV level. This is a short description of the laser wake field acceleration [18] (**Figure 17(a)**). Recent experiments using the laser wake field acceleration showed the quasimonoenergetic multi-GeV electron beams by focusing petawatt laser pulses [19–21]. The acceleration of electrons to 10 GeV or even 100 GeV level is now being pursued for the development of a compact electron accelerator.

Protons are also accelerated by a high-power laser pulse. In this case, a high-power laser pulse is focused onto a solid target. When a high-power laser pulse is focused on a thin metal target, the target immediately turns into plasma, and electrons in the plasma are accelerated toward the laser beam propagation direction by the ponderomotive force. Then there exists an electric field between accelerated electrons and background ions. The electric field can be used to accelerate protons existing in the metal as impurities [22, 23] (**Figure 17(b)**). At a lower laser intensity, the energy distribution for electrons is broad and the resultant proton energy distribution is also broad. As the laser intensity increases, proton energy distribution can be reduced by a narrow electron energy distribution by the radiation pressure. This is an indirect proton acceleration using electron acceleration. Protons can be directly accelerated to the light speed by an electromagnetic field as shown in Eq. (45). However, because of the proton mass, reaching to the speed of light by directly accelerating proton with an electromagnetic field requires a higher laser intensity up to ~$10^{24}$ W/cm$^2$, which is sometimes called the ultrarelativistic laser intensity. One of the ways for efficiently reaching at the ultrarelativistic laser intensity is to employ a tight focusing scheme. Based on the recent progress in the high-power laser, the demonstration of ultrarelativistic laser intensity will be possible soon.

Energetic charged particles driven by high-power laser pulses are directly used for medical applications including radiation therapy and imaging. For example, energetic proton beams having an energy range of 100–200 MeV can be used for the radiation tumor therapy [24]. When proton beams is irradiated to tumors in human body, protons dramatically lose their energy and produce x-rays in the tumor. The produced x-ray destroys DNA chains in a tumor cell and eventually kills the tumor cell. Electron beams with an energy range of 6–20 MeV can also be used for treating cancers locating at skin and lip, chest-wall and neck, respiratory and digestive-track lesions, or lymph nodes [25]. Research on stable and reliable production of energetic particles is of great interest for developing a compact particle accelerator for medical applications.

http://dx.doi.org/10.5772/64526

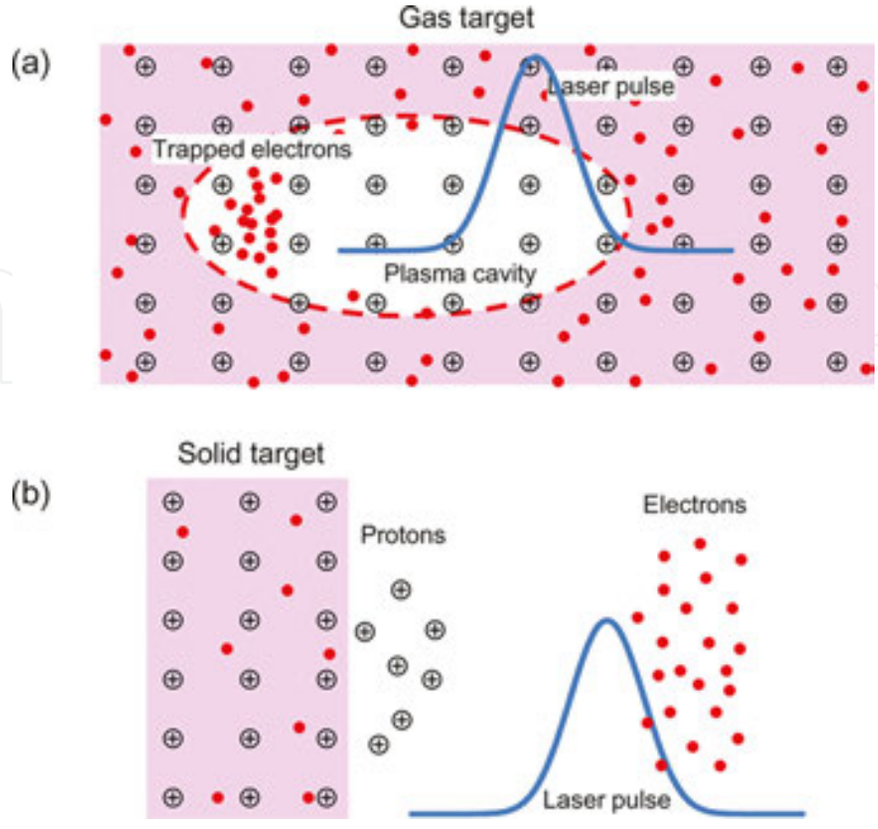


**Figure 17.** (a) Electron acceleration though the laser wake field. The laser pulse is focused onto the gas target. The electrons are captured in the plasma cavity and accelerated by the cavity. (b). Proton acceleration. The accelerated electrons by the laser pulse pull proton on the metal surface.

High-brightness and high-energy photons (x-ray and $\gamma$-ray) can be produced through the laser-plasma accelerator as well. By comparing to the large-scale facilities, such as synchrotron and XFEL, the laser-plasma accelerator produces high-energy photon providing an attosecond temporal resolution and subatomic spatial resolution in a small size and reasonable cost. High-energy photon can be used for research pertaining to ultrafast electron dynamics in atoms, molecules, plasmas, and solids. In the laser-plasma accelerator, many processes producing energetic photon sources, such as high harmonic generation [26], undulator radiation [27], betatron radiation [28], and Compton scattering [29], were proposed and some of them have been experimentally demonstrated. So far, basic applications for high-intensity laser pulses were described. Other interesting research topics related to fundamental physical processes are well described elsewhere [30].

## 5. Conclusion

The high-power laser facility is being developed for performing research on the laser-matter interaction in the relativistic and ultrarelativistic intensity regimes. The high-power laser pulse immediately ionizes solid and gas targets and makes the target medium plasma. The intensity

can make use of the laser pulse as a small-scale and versatile particle accelerator. This is a primary purpose for developing high-intensity laser facilities. The interaction between an intense laser pulse and energetic charged particles produces high-energy photon as well. Many interesting schemes, such as undulator radiation, betatron radiation, and inverse Compton scattering, have been studied for producing high-energy photons. The high-energy photons can be used in many disciplines including industrial application, medical imaging, nuclear engineering, national security, and so on. As the intensity obtainable with the high-power laser pulse increases over $10^{24}$ W/cm$^2$, some of the fundamental physical processes can be investigated by light pulses with an ultrashort time scale. Since the invention of laser, the application field of laser has been dramatically expanded as the laser intensity increases. Now, the acceleration of charged particle by intense coherent light field became possible in the relativistic laser intensity regime, and new era for studying the laser-plasma interaction in the ultrarelativistic laser intensity regime will be open soon.

## Author details

Tae Moon Jeong and Jongmin Lee*

*Address all correspondence to: leejm@gist.ac.kr

Handong Global University, Pohang, Republic of Korea

## References

[1] L. E. Hargrove, R. L. Fork, and M. A. Pollack. Locking of He-Ne laser modes induced by synchronous intracavity modulation. Appl. Phys. Lett. 1964;5(1):4–5.

[2] C. V. Shank and E. P. Ippen. Subpicosecond kilowatt pulses from a mode-locked cw dye laser. Appl. Phys. Lett. 1974;24(8):373–375.

[3] U. Morgner, F. X. Kartner, S. H. Cho, Y. Chen, H. A. Haus, J. G. Fujimoto, E. P. Ippen, V. Scheuer, G. Angelow, and T. Tschudi. Sub-two-cycle pulses from a Kerr-lens mode-locked Ti:sapphire laser. Opt. Lett. 1999;24:411–413.

[4] R. Paschotta and U. Keller. Passive mode locking with slow saturable absorbers. Appl. Phys. B. 2001;73:653–662. DOI: 10.1007/s003400100726

[5] O. Svelto. Principles of Lasers. 4th ed. New York: Springer; 1998. 343 pp.

[6] H. A. Haus, J. G. Fujimoto, and E. P. Ippen. Structures for additive pulse mode locking. J. Opt. Soc. Am. B. 1991;8(10):2068–2076. DOI: 10.1364/JOSAB.8.002068

[7] D. E. Spence, D. E. Kean, and W. Sibbet. 60-fsec pulse generation from a self-mode-locked Ti:sapphire laser. Opt. Lett. 1991;16:42–44.

[8] D. Strickland and G. Mourou. Compression of amplified chirped optical pulses. Opt. Commun. 1985;6:219–221.

[9] T. M. Jeong and J. Lee. Femtosecond petawatt laser. Ann. Phys. (Berlin). 2014;526(3–4): 157–172. DOI: 10.1002/andp.201300192

[10] E. Treacy. Optical pulse compression with diffraction gratings. IEEE J. Quantum Electron. 1969;5(9):454–458. DOI: 10.1109/JQE.1969.1076303

[11] O. Martinez. 3000 times grating compressor with positive group velocity dispersion: application to fiber compensation in 1.3–1.6 μm region. IEEE J. Quantum Electron. 1987;23(1):59–64. DOI: 10.1109/JQE.1987.1073201

[12] L. M. Frantz and J. S. Nodvik. Theory of pulse propagation in a laser amplifier. J. Appl. Phys. 1963;34(8):2346–2349.

[13] M. D. Perry, D. Pennington, B. C. Stuart, G. Tietboh, J. A. Britten, C. Brown, S. Herman, B. Golick, M. Kartz, J. Miller, H. T. Powell, M. Vergino, and V. Yanovsky. Petawatt laser pulses. Opt. Lett. 1999; 24(3):160–162.

[14] J. H. Sung, S. K. Lee, T. J. Yu, T. M. Jeong, and J. Lee. 0.1 Hz 1.0 PW Ti:sapphire laser. Opt. Lett. 2010;35(18):3021–3023.

[15] Y. Chu, Z. Gan, X. Liang, L. Yu, X. Lu, C. Wang, X. Wang, L. Xu, H. Lu, D. Yin, Y. Leng, R. Li, and Z. Xu. High-energy large-aperture Ti:sapphire amplifier for 5 PW laser pulses. Opt. Lett. 2010;40(21):5011–5014.

[16] J. Stratton and L. Chu. Diffraction theory of electromagnetic waves. Phys. Rev. 1939;56(1):99–107.

[17] T. M. Jeong, S. Weber, B. Le Garrec, D. Margarone, T. Mocek, and G. Korn. Spatio-temporal modification of femtosecond focal spot under tight focusing condition. Opt. Express. 2015;23(9):11641–11656 . DOI: 10.1364/OE.23.011641

[18] T. Tajima and J. M. Dawson. Laser electron accelerator. Phys. Rev. Lett. 1979;43(4):267–270.

[19] N. M. Hafz, T. M. Jeong, I. W. Choi, S. K. Lee, K. H., Pae, V. V. Kulagin, J. H. Sung, T. J. Yu, K.-H. Hong, T. Hosokai, J. R. Cary, D.-K. Ko, and J. Lee. Stable generation of GeV-class electron beams from self-guided laser–plasma channels. Nat. Photon. 2008;2:571–577.

[20] H. T. Kim, K. H. Pae, H. J. Cha, I. J. Kim, T. J. Yu, J. H. Sung, S. K. Lee, T. M. Jeong, and J. Lee. Enhancement of electron energy to the multi-GeV regime by a dual-stage laser-Wakefield accelerator pumped by petawatt laser pulses. Phys. Rev. Lett. 2013;111(16): 165002.

[21] W. P. Leemans, A. J. Gonsalves, H.-S. Mao, K. Nakamura, C. Benedetti, C. B. Schroeder, C. Tóth, J. Daniels, D. E. Mittelberger, S. S. Bulanov, J.-L. Vay, C. G. R. Geddes, and E.

Esarey. Multi-GeV Electron beams from capillary-discharge-guided subpetawatt laser pulses in the self-trapping regime. Phys. Rev. Lett. 2014;113(24):245002.

[22] S. P. Hatchett, C. G. Brown, T. E. Cowan, E. A. Henry, J. S. Johnson, M. H. Key, J. A. Koch, A. B. Langdon, B. F. Lasinski, R. W. Lee, A. J. Mackinnon, D. M. Pennington, M. D. Perry, T. W. Phillips, M. Roth, T. C. Sangster, M. S. Singh, R. A. Snavely, M. A. Stoyer, S. C. Wilks, and K. Yasuike. Electron, photon, and ions beams from the relativistic interaction of Petawatt laser pulses with solid targets. Phys. Plasma. 2000;7(5):2076–2082.

[23] A. Macchi, F. Cattani, T. V. Liseykina, and F. Cornolti. Laser acceleration of ion bunches at the front surface of overdense plasmas. Phys. Rev. Lett. 2005;94:165003.

[24] S. V. Bulanov and V. S. Khoroshkov. Feasibility of using laser ion accelerators in proton therapy. Plasma Phys. Rep. 2002;28:453–456.

[25] K. R. Hogstrom and P. R. Almond. Review of electron beam therapy physics. Phys. Med. Biol. 2006;51:R455–R489. DOI: 10.1088/0031-9155/51/13/R25

[26] I. J. Kim, K. H. Pae, C. M. Kim, H. T. Kim, H. Yun, S. J. Yun, J. H. Sung, S. K. Lee, J. W. Yoon, T. J. Yu, T. M. Jeong, C. H. Nam, and J. Lee. Relativistic frequency upshift to the extreme ultraviolet regime using self-induced oscillatory flying mirrors. Nat. Commun. 2012;3:1231. DOI: 10.1038/ncomms2245

[27] M. Fuchs, R. Weingartner, A. Popp, Z. Major, S. Becker, J. Osterhoff, I. Cortrie, B. Zeitler, R. Hörlein, G. D. Tsakiris, U. Schramm, T. P. Rowlands-Rees, S. M. Hooker, D. Habs, F. Krausz, S. Karsch, and F. Grüner. Laser-driven soft-X-ray undulator source. Nat. Phys. 2009;5:826–829. DOI: 10.1038/NPHYS1404

[28] A. Rousse, K. Ta Phuoc, R. Shah, A. Pukhov, E. Lefebvre, V. Malka, S. Kiselev, F. Burgy, J.-P. Rousseau, D. Umstadter, and D. Hulin. Production of a keV X-ray beam from synchrotron radiation in relativistic laser-plasma interaction. Phys. Rev. Lett. 2004;93:135005.

[29] N. D. Powers, I. Ghebregziabher, G. Golovin, C. Liu, S. Chen, S. Banerjee, J. Zhang, and D. P. Umstadter. Quasi-monoenergetic and tunable X-rays from a laser-driven Compton light source. Nat. Photon. 2014;8:28–31. DOI: 10.1038/NPHOTON.2013.314

[30] G. Mourou, T. Tajima, and S. Bulanov. Optics in the relativistic regime. Rev. Mod. Phys. 2006;78:309–371.